MIC based Photovoltaic Integrated Grid Topology with Energy Buffer

G.Vasundra[1] P.M.Rupa[2] V.Hari Babu[3]
[1]P.G. Student [2]Assistant Professor [3]Associate Professor & Head of Dept.
[1,2,3]Department of Electrical & Electronics Engineering
[1,2,3]Prakasam Engineering College, Kandukur, AP., India

Abstract— *The growing power demand brings drastic changes in grid topologies, where renewable source integration provides pollution less power. This paper provides renewable source integrating topology. This introduces a new topology that places the energy storage block in a series-connected path with the line interface block. This design provides independent control over the capacitor voltage, soft-switching for all semiconductor devices, and the full four-quadrant operation with the grid. The proposed system is studied with MATLAB/SIMULINK environment.*

Keywords— Distributed Power Generation, Grid-Connected PV Systems, High-Frequency AC-Link, Module Integrated Converter (MIC), Multiport Circuit, Photovoltaic (PV) Inverter, Photovoltaic Power Systems, Resonant Power Converters, Single-Phase Energy Storage, Single-Phase Inverters, Single-Stage Inverters, Switching Circuits, Zero Voltage Switching

I. INTRODUCTION

Grid Connected inverters for photovoltaic systems represent a rapidly developing area. Module-integrated converters (MICs), sometimes known as micro inverters, are designed to interface a single, low-voltage (25–40 V, typically) panel to the ac grid [1]–[5]. Such converters provide a number of benefits: ease of installation, system redundancy, and increased energy capture in partially shaded conditions [6].

MICs typically target single-phase electrical systems [7] (e.g., at 240 V), and are typically restricted to the unity power factor operation [8]. Therefore, the converter must deliver average power plus a time-varying power component at twice the line frequency, while drawing a constant power from the PV mod-ule. Fig. 1 illustrates the power transfer versus time for the grid and the PV module, with the shaded area between the curves indicating the temporal energy storage required for the inverter. To model this transfer of energy through the converter, a generalized three-port system can be used.

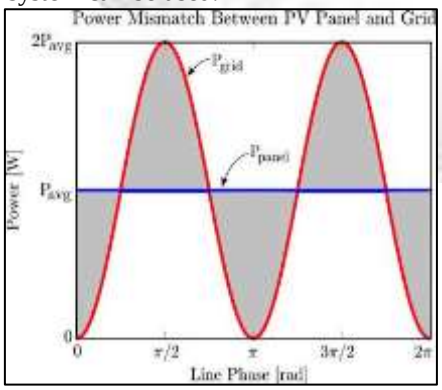

Fig. 1: Power flow mismatch between the grid and a constant power source results in the shaded area, representing the required energy storage.

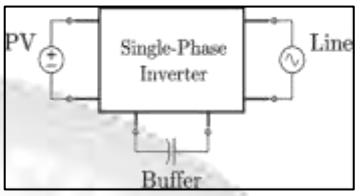

Fig. 2: Generalized grid-connected power converter, visualized as a three-port system

The constant power source of the PV and the sinusoidal power load of the grid are illustrated in Fig. 2, and can be written as

$$P_{PV} = P_{avg} \quad (1)$$

$$PLine = - P_{avg} (1- coss(2wt) \quad (2)$$

When no reactive power is transferred. The energy storage buffer must absorb and deliver the difference in power between these two ports, specifically

$$P_{Buf} = - P_{avg} \cos(2wt) \quad (3)$$

Inverters investigated in the past (see the literature reviews [4], [5]) can be classified by the location and the operation of the energy storage buffer within the converter. Most single-stage topologies, such as fly back and ac-link converters, place capacitance in parallel with the PV panel [9], [10]. This is an effective low-complexity implementation, but to avoid interfering with the maximum peak-power tracking (MPPT) efficiency, substantial energy storage is required to limit the voltage ripple across the panel. A second common method involves two complete cascaded conversion stages, providing energy storage at an intermediate dc bus. This arrangement can be implemented with less energy storage than the previous method, as a larger voltage fluctuation on the intermediate bus can be tolerated without impacting the MPPT operation. The removal of the energy storage from the input also improves the transient response for peak-power tracking, as the PV module voltage can be controlled with a much higher bandwidth One drawback common to both of the energy storage methods described previously involves the typical use of electrolytic capacitors for the dc energy storage. Electrolytic capacitors are traditionally selected due to their high energy density, but suffer from the stigma of long-term failure rates.

As MICs are typically mounted on the frame or back sheet of the PV module assembly, the high temperatures can accelerate aging processes for many of the internal components. To address this, focus is placed on improving converter efficiency (i.e., reduction in thermal output) and transitioning to the use of higher-reliability capacitors. Recent developments in converter topologies have included “third-port” systems [11], [12], providing active con-trol of the energy storage stage, independent of the input and output voltages. This reduces the required energy storage, and provides the opportunity for less energy-dense film capacitors to be used.

The power converter presented in this paper implements a new type of third-port topology, where the energy storage (buffer) block is placed "in series" with the line voltage interface. The topology achieves high efficiencies with its continuous constant-power operation, zero-voltage switching (ZVS) capability for all devices, and reduced volt-seconds applied to the high-frequency transformer.

II. PROPOSED SOLUTION

The block diagram and schematic in Fig. 3 illustrate the four functional blocks of the converter: the high-frequency resonant inverter, transformation stage, energy buffer, and cycloconverter. Each is connected electrically in series, with a common high-frequency resonant current linking them together.

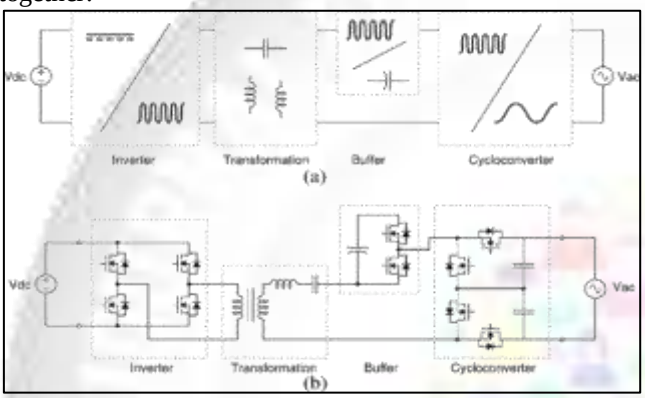

Fig. 3: Proposed photovoltaic module-integrated converter: (a) block diagram and (b) schematic.

At first glance, this series-connected configuration would seem to impose a heavy conduction-loss penalty. However, scaling up device sizes appropriately can reduce this impact, and the switching losses associated with large MOSFET devices can be greatly reduced through soft-switching techniques [13].

Additionally, the resistive channel structure allows current to flow both directions through the device, allowing for bidirectional power flow in each block of the converter. This is in contrast with devices such as IGBTs, SCRs, and diodes which allow current flow in a single direction and impose a fixed on-state voltage drop. Additionally, the figure-of-merit for MOS-FETs has improved steadily since their introduction, particularly with the recent charge-compensation principles. This has allowed high-voltage silicon MOSFETs to surpass the "silicon limit" [14]–[16] and become viable for voltage ranges once relegated to low-frequency IGBTs. Additionally, the emergence of wide-band gap FET-based device structures, implemented in SiC and GaN, have the potential to meet these same voltage levels while dramatically reducing the on-state resistance and undesirable device parasitics [17], [18]. This historical semiconductor device progress, combined with these and other anticipated future developments, are a motivating factor in the elimination of p-n junction devices in the topology. This study shows that this approach provides high efficiency with presently available de-vices, and is anticipated to scale with the improvements in device technology. Even with the departure from traditional converter design, the well-known methods and algorithms for MPPT [19], grid synchronization [20], and islanding detection [21] can continue to be used.

A. Solar Unit

The Renewable Source unit provides the required real power during the compensation of voltage sag. Generally super capacitors, fly wheels, lead acid batteries are used as batteries for supplying the required amount of power. Here the model proposes to utilize the available renewable source in effective manner. The required amount of energy demand depends on voltage abnormality, load MVA requirement and control strategy applied.

Many MPPT algorithms have been proposed in literature. Mostly used techniques are Perturbation & Observation (P&O) and Incremental conductance. P&O method is widely used due to simple feedback and fewer parameters. The Solar Unit consists of PV cell Maximum Power Point Tracking unit (MPPT) and DC-DC converter. The model of solar cell is shown in Figure 5.

Here the solar unit is designed with MPPT which produces maximum output power.

$$P_p = V_p * I_p \qquad (4)$$

The terminal current and voltage of solar cell are given by,

$$I_p = I_{sc} - I_{sat}\{\exp[\frac{q}{AkT}(V_p + I_p R_{se}) - 1]\} - \frac{V_p + I_{sc} R_{se}}{R_{sh}} \qquad (5)$$

$$V_p = \frac{AkT}{q} \ln\{\frac{I_{sc}}{I_p} + 1\} \qquad (6)$$

Here R_{se} is series resistance, R_{sh} is shumt resistance, k is Boltzmann constant and Diode Ideality factor is A.

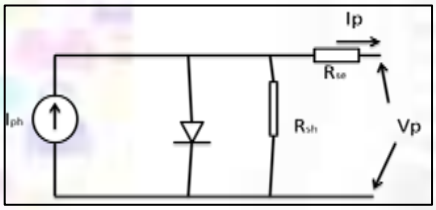

Fig. 4: Solar Cell unit equivalent Circuit.

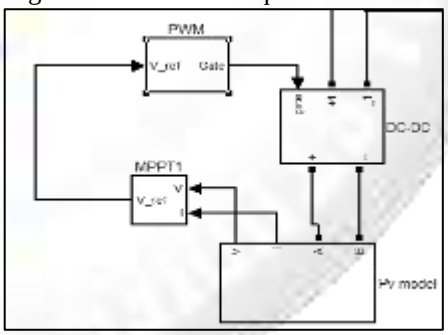

Fig. 5: Solar Unit

The MPPT based Solar cell Unit output is connected to the DC-DC converter in order to maintain the constant voltage at DC link of the inverter.

III. TOPOLOGY OPERATION AND ANALYSIS

At a very high level, the converter operation is closely re-lated to the ac-link family of topologies. Here, the switching waveforms of all three series-connected blocks are responsible for generating the intermediate high-frequency current wave-form. This can be seen in Fig. 6, where each active switching block is replaced with an idealized square-

wave voltage source, and connected in series with the resonant circuit. To modulate power flow through the converter, each block uses the resulting series current as a reference, to which it readjusts its switching waveform appropriately.

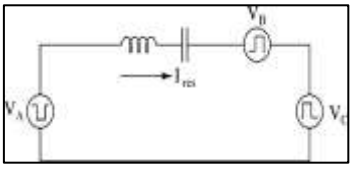

Fig. 6: Proposed topology of Fig. 3, where each active switching block is replaced with a square-wave voltage source. The applied voltage of all three blocks results in a high-frequency series current which links each block together

The interdependence of the resonant current and switching behavior of the three blocks presents a challenge for directly evaluating the full converter operation. To ease this, the analysis is performed with two simplifying approximations: 1) the quality factor of the series resonant circuit is sufficiently high to approximate it as a sinusoidal current source operating at the switching frequency; and 2) the voltage at each terminal of the converter (PV, buffer, and line) changes slowly enough, relative to the switching frequency, that they can be approximated as constant over a switching cycle.

With these, the converter can then be decoupled into the two circuits in Fig. 7, separated such that the dc-connected inverter and transformation blocks are grouped into the primary side, and the buffer and cyclo converter are grouped into the secondary side. This permits the two circuits to be analyzed separately, which motivates the design process outlined in this section.

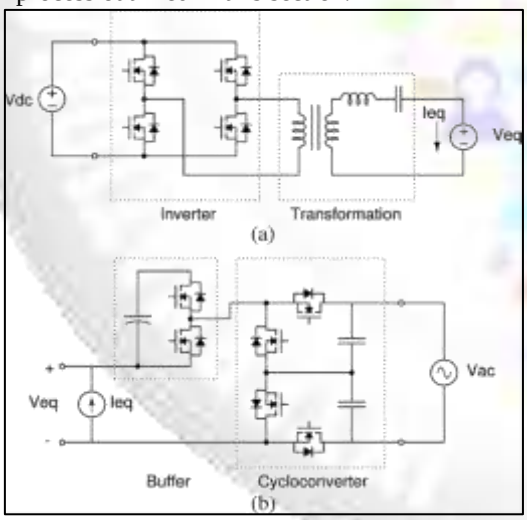

Fig. 7: Equivalent circuits representing the (a) primary and (b) secondary sides, decoupled by approximating the output of the transformation stage as a current source.

A. Switch Modulation

Both the primary and secondary sides of the converter are constructed from a number of canonical totem-pole structures. The buffer is composed of one such block, where the energy storage voltage is represented as unipolar, while the line-interfaced cycloconverter is composed of two such blocks, in a common-source layout (each providing operation under opposite voltage polarities).

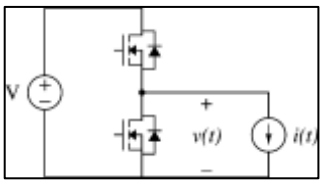

Fig. 8: Constituent sub circuit of the buffer and cycloconverter blocks from Fig. 5(b).

The modulation of power through the simple circuit in Fig. 8 is accomplished by controlling the switching of the voltage waveform $v(t)$ relative to the series resonant current $i(t)$.

B. Resonant Current Magnitude

In addition to the switching parameters, the resonant cur-rent magnitude remains as an additional parameter for modulating the power transfer through the converter. For each block, a lower bound exists on the required magnitude of cur-rent needed to achieve a desired power transfer. As the terminal voltages V and resonant current magnitude I of the canonical circuit in Fig. 6 vary slowly over a line cycle, the defined power flow requirements in (1)–(3) result in the minimum current pro-files shown in Fig. 9. For this case, the buffer-block voltage is assumed to be constant, such that the peak current requirements of I_B and I_C are equal.

Operating with the minimum resonant current may be desirable to limit conduction losses; however, the selection of cur-rent magnitude directly impacts the resulting converter control parameters. When operating with a fixed duty cycle, and implementing simple phase-shift control, the required phase-angle for each block are given by,

$$\Theta_c(t) = \pm \cos^{-1} \frac{\Pi Ic\ Sin(wt)}{I_r\ (wt)} \quad (7)$$

$$\Theta_B(t) = \pm \cos^{-1} \frac{\Pi Ic\ Sin(wt)}{I_r\ (wt)} \quad (8)$$

Where θC and θB are the phase angle parameters for the cycloconverter and buffer blocks, respectively, IC and IB are the corresponding peak current requirements, and Ir (t) is the resonant current amplitude. Each phase expression is symmetric and contains two valid solutions, allowing a choice based on an external constraint or preference (e.g., ZVS).

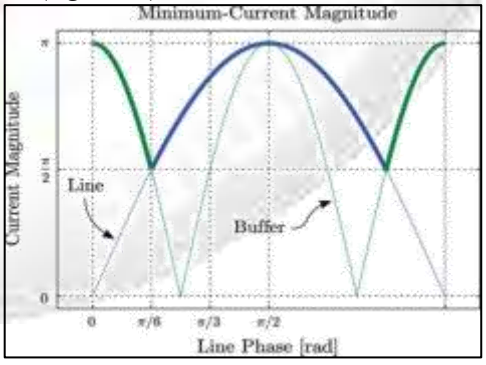

Fig. 9: Minimum resonant current magnitude requirements for the buffer block and cycloconverter, including the bold line indicating the envelope of current that meets both constraints.

C. Transformation and Inverter Design

With an understanding of the behavior of the secondary side of the converter, the primary-side circuit in Fig. 5(a) can be

considered with the objective of obtaining an inverter and transformation combination capable of synthesizing the required resonant current, as defined in the preceding section. The transformation stage is designed to provide impedance appropriate for the primary side driving circuit; in this case it is desired to present a positive reactance at the switching frequency for the bridge converter to achieve the desired ZVS conditions. Additionally, the magnitude of the impedance must be managed such that the inverter is capable of operating over the full required voltage and power range. The varying control and behavior of the secondary half of the converter results in a dynamic load over a line cycle. Using phasors, the secondary-side circuit can be approximated as complex impedance at the switching frequency, as shown in Fig. 10. The equivalent impedance is calculated using

$$Z = \frac{V_C + V_B}{I} \qquad (9)$$

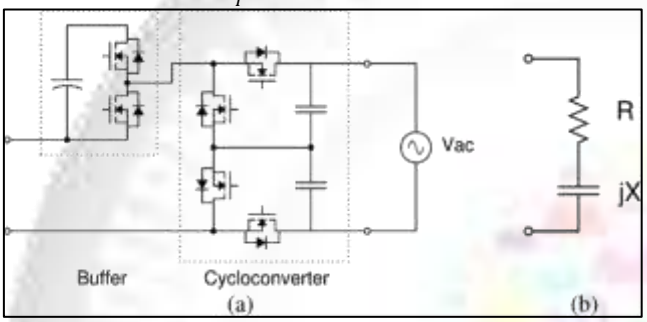

Fig. 10: (a) Buffer block and cycloconverter can be approximated as (b) the complex load impedance.

To drive this compensated load, the inverter is operated as a phase-shift full-bridge, where its applied voltage is defined in phasor form as where δ represents the duty cycle and θ is the phase of the voltage relative to the resonant current waveform. With control of this driving voltage, and the flexibility in selecting the transformer turns ratio and the resonant tank component values, a transformation stage and inverter can be created which is capable of synthesizing the required resonant current.

IV. SIMULATION RESULTS

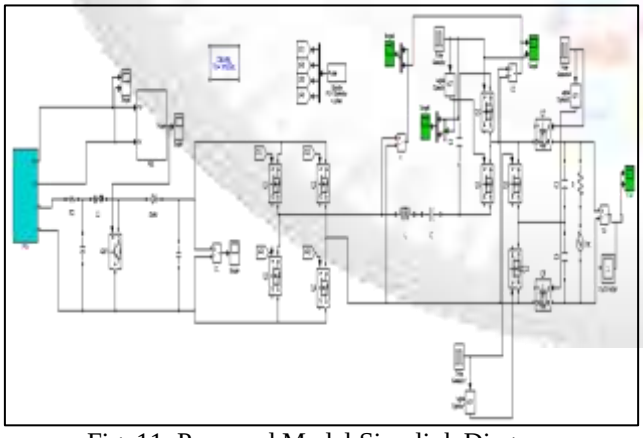

Fig. 11: Proposed Model Simulink Diagram

The proposed energy buffer system simulink model is as shown in Fig. 11The model is fed with P & O algorithm based MPPT –PV system. Fig 12 shows the output voltage and current waveforms of PV system. The PV output voltage is maintained almost at constant value.

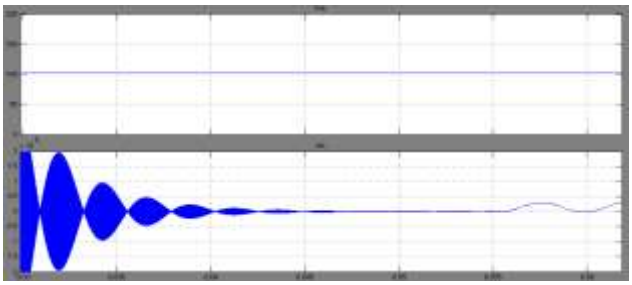

Fig. 12: PV Output Voltage and Currents

The input and output of the series connected buffer circuit is as show in Fig. 13.

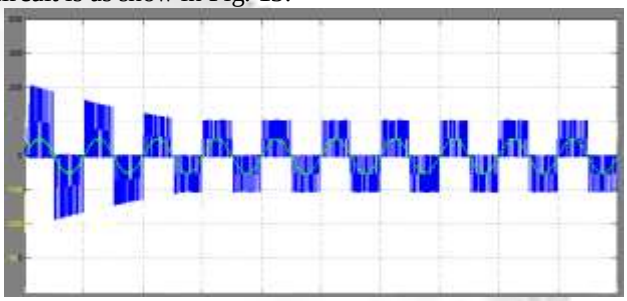

Fig. 13: Constituent subcircuit of the buffer and cycloconverter blocks from Fig. 5(b).

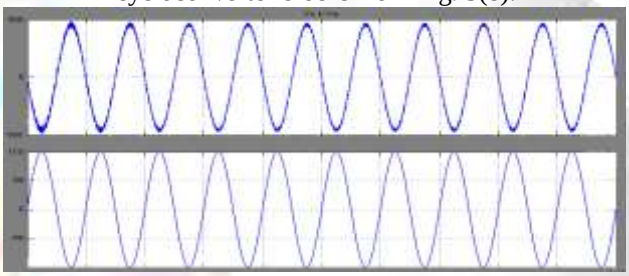

Fig. 14: Increased Terminal Voltage and actual input voltage.

Fig. 14 Gives clear outcome of the proposed model. Here due to the buffer circuit the output voltage has been improved. The % THD of the Voltage is maintained as per IEEE standards below4%.This is shown in Fig 15.

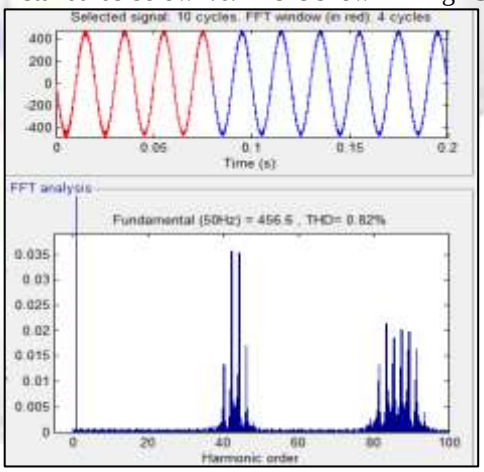

Fig. 8: Constituent subcircuit of the buffer and cycloconverter blocks from Fig. 5(b).

V. CONCLUSION

The converter design presented in this paper has demonstrated a novel topology with an energy-storage buffer in the series-connected path with the line interface. It has an increased complexity relative to traditional designs,

but allows control over the energy storage voltage and ripple. It also maintains the capability of reactive power transfer and high efficiency.

The presented bench prototype maintains the % THD below 4% and improves output. Further improvements on these successful results are expected with optimized magnetics and online tuning of control parameters.

REFERENCES

[1] H. Haeberlin, "Evolution of inverters for grid connected PV-systems from 1989 to 2000," Measurement, 2:1, presented at the 17th Eur. Photovoltaic Solar Energy Conf., Munich, Germany, Oct. 26, 2001

[2] S. B. Kjaer, J. K. Pedersen, and F. Blaabjerg, "A review of single-phase grid-connected inverters for photovoltaic modules," IEEE Trans. Ind. Appl., vol. 41, no. 5, pp. 1292–1306, Sep./Oct. 2005.

[3] S. B. Kjaer, J. K. Pedersen, and F. Blaabjerg, "Power inverter topologies for photovoltaic modules-a review," in Proc. 37th IAS Annu. Ind. Appl. Conf. Meet. Rec., 2002, vol. 2, pp. 782–788.

[4] Y. Xue, L. Chang, S. B. Kjaer, J. Bordonau, and T. Shimizu, "Topolo-gies of single-phase inverters for small distributed power generators: An overview," IEEE Trans. Power Electron., vol. 19, no. 5, pp. 1305–1314, Sep. 2004.

[5] Q. Li and P. Wolfs, "A review of the single phase photovoltaic module integrated converter topologies with three different dc link configurations," IEEE Trans. Power Electron., vol. 23, no. 3, pp. 1320–1333, May 2008.

[6] E. Roman, R. Alonso, P. Ibanez, S. Elorduizapatarietxe, and D. Goitia, "Intelligent PV module for grid-connected PV systems," IEEE Trans. Ind. Electron., vol. 53, no. 4, pp. 1066–1073, Jun. 2006.

[7] A. Lohner, T. Meyer, and A. Nagel, "A new panel-integratable inverter concept for grid-connected photovoltaic systems," in Proc. IEEE Int. Symp. Ind. Electron., Jun. 1996, vol. 2, pp. 827–831.

[8] Inverters, Converters, Controllers and Interconnection System Equipment for Use With Distributed Energy Resources, UL, ISO 1741., 1999

[9] A. Trubitsyn, B. J. Pierquet, A. K. Hayman, G. E. Gemache, C. R. Sullivan, and D. J. Perreault, "High-efficiency inverter for photo-voltaic applications," in Proc. IEEE Energ. Convers. Congr. Expo., Sep. 2010, pp. 2803–2810.

[10] Q. Mo, M. Chen, Z. Zhang, Y. Zhang, and Z. Qian, "Digitally controlled active clamp interleaved flyback converters for improving efficiency in photovoltaic grid-connected micro-inverter," in Proc. 27th Annu. IEEE Appl. Power Electron. Conf. Expo., Feb. 2012, pp. 555–562.

[11] P. T. Krein and R. S. Balog, "Cost-effective hundred-year life for single-phase inverters and rectifiers in solar and led lighting applications based on minimum capacitance requirements and a ripple power port," in Proc. 24th Annu. IEEE Appl. Power Electron. Conf. Expo., Feb. 2009, pp. 620–625.

[12] B. R. Bush and B. Wang, "A single-phase current source solar inverter with reduced-size DC link," in Proc. IEEE Energ. Convers. Congr. Expo., Sep. 2009, pp. 54–59.

[13] A P. Henze, H. C. Martin, and D. W. Parsley, "Zero-voltage switching in high frequency power converters using pulse width modulation," in Proc. 3rd Annu. IEEE Appl. Power Electron. Conf. Expo., Feb. 1988, pp. 33–40.

[14] K. Sheng, F. Udrea, G. A. J Amaratunga, and P. R Palmer, "Unconven-tional behaviour of the CoolMOS device," in Proc. Eur. Solid-State Dev. Res. Conf., Nuremberg, Germany, 2001, pp. 251–254.

[15] L. Lorenz, G. Deboy, A. Knapp, and M. Marz, "COOLMOS TM—A new milestone in high voltage power MOS," in Proc. 11th Int. Symp. Power Semicond. Devices,, 1999, pp. 3–10.

[16] L. Lorenz, I. Zverev, A. Mittal, and J. Hancock, "CoolMOS—A new ap-proach towards system miniaturization and energysaving," in Proc. IEEE Ind. Appl. Conf. Rec., 2000, vol. 5, pp. 2974–2981.

[17] J. A Cooper Jr., M. R Melloch, R. Singh, A. Agarwal, and J. W Palmour, "Status and prospects for SiC power MOSFETs," IEEE Trans. Electron. Devices, vol. 49, no. 4, pp. 658–664, Apr. 2002.

[18] B. J. Baliga, "Trends in power semiconductor devices," IEEE Trans. Elec-tron. Devices, vol. 43, no. 10, pp. 1717–1731, Oct. 1996.

[19] T. Esram and P. L. Chapman, "Comparison of photovoltaic array max-imum power point tracking techniques," IEEE Trans. Energ. convers., vol. 22, no. 2, pp. 439–449, Jun. 2007.

[20] F. Blaabjerg, R. Teodorescu, M. Liserre, and A. V. Timbus, "Overview of control and grid synchronization for distributed power generation sys-tems," IEEE Trans. Ind. Electron., vol. 53, no. 5, pp. 1398–1409, Oct. 2006.